Surface-barrier reflection of diffusing positrons

G. R. Brandes*
Department of Physics, Brandeis University, Waltham, Massachusetts 02254
(Received 26 September 1990)

The reemitted positron yield from a 1500-Å-thick Ni(100) foil was measured as a function of incident positron energy. The magnitude of the positron internal surface reflection coefficient, $\mathcal{R}=0.63\pm0.04$, was determined by fitting calculated positron yields to the data. This value agrees with the value calculated using the one-dimensional, potential-step model advanced by Britton *et al.* [Phys. Rev. Lett. **62**, 2413 (1989)]. The mean positron penetration depth varies with incident positron energy as $\bar{z}=\alpha E^n$, where α is fixed ($\alpha=400/\rho$ Å/keV^n, ρ is the sample density in g cm^{-3}) and $n=1.61\pm0.03$, in good agreement with positron back-reemission measurements from thick single crystals.

I. INTRODUCTION

The motion of a positron in a solid, once it has lost its implantation kinetic energy and has reached thermal equilibrium with the surrounding material, is well described by the positron diffusion equation.[1,2] If the material has a negative positron work function, the boundary (surface) is usually treated as perfectly absorbing,[3] that is, the probability of the positron being internally reflected at the surface is zero. However, Britton *et al.*[4] recently demonstrated that positron and positronium (e^--e^+ bound state) yields are greatly reduced as the sample temperature is lowered and vanish at $T=0$ K. Their data were consistent with a quantum-mechanical reflection of the positron wave function from the surface potential.[5,6] The positron-surface interaction was adequately modeled as a simple one-dimensional barrier problem, the positron wave function was described as a plane wave, and the potential at the surface as a step function. While their results demonstrated the relative reflection temperature dependence predicted by this model, the probability that the positron is internally reflected, i.e., the magnitude of $\mathcal{R}$, could not be obtained. In this paper $\mathcal{R}$ for Ni(100) is determined from comparing reemitted transmitted positron yield data from a thin single crystal with slow positron yields calculated with the positron diffusion equation and a reflective boundary condition. Also, analyzing the variation of the transmitted positron yield with incident positron energy,[7] instead of the bulk crystal, back-reemitted positron yield,[1] provides an additional way to examine the energy-dependent positron implantation or stopping profile.

The experiment consisted of focusing an intense, small-diameter positron beam[8] onto a thin (1500 Å) Ni single crystal. The reemitted positron yield at the opposing surface of the Ni foil was measured as a function of implantation energy with a positron reemission microscope (PRM), which images reemitted positrons, as originally proposed by Hulett *et al.*[9] Our PRM operates in the transmission mode;[10] a reflection mode PRM was constructed and operated by van House and Rich.[11] There are two advantages to this experimental approach. Unlike backscattering measurements, below a certain implantation energy, effectively all positrons emitted from the opposing surface have thermalized and there is no appreciable nonthermal background to complicate the analysis. Schultz *et al.*[12] investigated the slow positron yield from a thin (1350±100 Å) Ni crystal with a large-diameter (1.2 or 2 mm) collimated beam. They found the maximum yield was high (19% at $E=5.0$ keV) and that there was a surprisingly large yield at low incident positron energy (1.3% at $E=24$ eV). They suggested the large, low-energy yield might be due to an effective nonzero positron implantation depth at very low energy or a large positron reflection coefficient at the diffusion boundary. There was a large degree of scatter in their data which they attributed to beam motion and sample nonuniformities. By measuring the yield with the PRM an image of the sample may be formed simultaneously and used to insure that the same sample region is illuminated each time a measurement is taken. Also, by using a few micrometer diameter beam it is possible to illuminate a smaller area with a corresponding reduction in the susceptibility to large scale foil inhomogeneities.

II. EXPERIMENTAL PROCEDURE

The sample was a free-standing Ni(100) crystal grown by evaporation on a NaCl crystal. The foil was floated off its substrate and tautly mounted by self-adhesion to a Ni disc with a 1-mm-diam hole.[13] The foil thickness w was measured to be 1500±50 Å.[14] In a separate vacuum chamber (5×10^{-9} torr), the foil was annealed at 900 °C for 10 m; the foil temperature was gradually reduced over a 15-m period. The foil was exposed to air for 1 h during transfer to the PRM. Once the microscope chamber was evacuated (10^{-10} torr after a 24 h, 150 °C bakeout), a low magnification PRM image of the sample was formed. The transport optics were tuned to focus the 3300 e^+ s^{-1} beam to the smallest possible spot at 1-keV incident beam energy (microbeam lens off). By increasing the potential difference between the microbeam lens electrodes (while keeping all other lens potentials fixed relative to the po-

tential of the first microbeam lens electrode), the energy of the incident beam could be varied. The positron microbeam centroid shifted less than 50 μm from the 1 keV position over the 1–5 keV energy range examined. A retuning of the beam at 5-keV incident energy yielded no more positrons.

The data were taken over a 12-h period. The incident beam energy was set (random order) and a 600-s PRM image was acquired. Following this, the incident beam was deflected away from the microbeam lens entrance (see Fig. 1). With the positron beam in this position, a 600-s PRM image was acquired to measure the PRM detector background and the beam annihilation γ's were measured to verify the stability of the incident beam flux with respect to incident energy. This process was repeated until the entire energy range was covered. The beam was periodically turned off at the second remoderator to get a second measurement of the PRM detector background and to determine the γ-ray background. No differences between the two different PRM detector background measurements outside of statistical fluctuations were observed. The absolute PRM detector efficiency, typically ~ 0.50 (Ref. 15) for 5-keV positrons, need not be known to determine the fraction of positrons reemitted. This is because the γ-ray detector (used to verify the incident beam stability) was calibrated relative to the PRM detector with the sample removed allowing 100% of the beam to reach the detector. The beam annihilation γ's were converted to channelplate counts and compared to the reemitted positron counts directly to determine the yield.

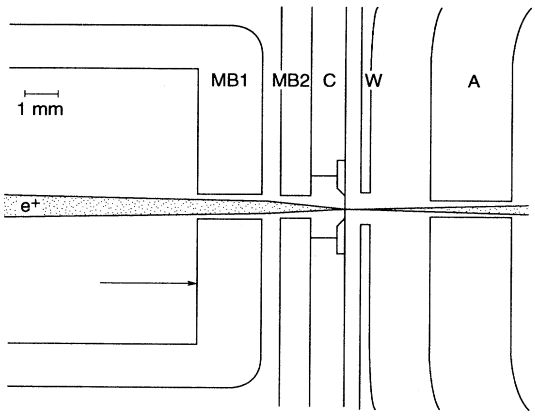

FIG. 1. Scale drawing of the central portion of the PRM microbeam lens and objective. The final acceleration and focusing of the incident positrons is performed by the microbeam lens (elements MB1 and MB2). The positrons strike the sample (shown as a thin line crossing the optical axis) and the remitted positrons are accelerated and focused by the objective lens [elements *C* (cathode), *W* (wehnelt), and *A* (anode)]. The incident beam stability and strength was determined by periodically deflecting the beam off axis to the region indicated by the arrow and monitoring the annihilation γ's.

III. RESULTS AND ANALYSIS

The results of the yield versus implantation energy investigation are shown in Fig. 2. The reduced scatter in the data as compared to Schultz *et al.*[12] makes the data more amenable to a quantitative modeling of the results. The fraction of thermal positrons leaving the sample through the imaged surface was calculated by numerically solving the one-dimensional positron diffusion equation:

$$\frac{\partial n(z,t)}{\partial t} = D_+ \frac{\partial^2 n(z,t)}{\partial z^2} - \frac{n(z,t)}{\tau} \ . \tag{1}$$

Here $n(z,t)$ is the positron density, D_+ is the positron diffusion constant, and $\tau = 100$ ps is the positron lifetime in well-annealed Ni.[16] The initial positron distribution (implantation profile) was characterized with the function[17]

$$P(z,E) = \frac{m z^{m-1}}{z_0^m} \exp\left[-\left[\frac{z}{z_0} \right]^m \right] , \tag{2}$$

where m is the shape parameter, $z_0 = \bar{z}/\Gamma(1+m^{-1})$ is the penetration parameter, $\bar{z} = \alpha E^n$ is the mean stopping depth, and E is the incident positron energy.[18] Theoretical and experimental investigations[1] typically yield implantation profile parameter values of $m \approx 2.0$, $n \approx 1.6$, and $\alpha \approx 400/\rho$ Å/keV^n, where ρ is the sample density (g cm^{-3}). The Crank-Nicholson technique[19] was used to solve the diffusion equation with (in most cases) a 25 Å cell size and a time step of 1×10^{-4} ps. The calculation was halted when fewer than 0.1% of the positrons remained in the crystal. When possible, the accuracy of the numerical solutions was verified by comparing it to results from analytical calculations. The discrepancy between analytical and numerical solutions was less than 4% of the calculated value.

The number of incident positrons implanted in the crystal is reduced due to backscattering from the crystal. Baker and Coleman[20] measured the positron backscattering fraction from Al, Cu, Ag, and W samples over a 0.5–30 keV incident positron energy range. Only backscattered positrons with energy greater than 10 eV were counted, although the epithermal[21,22] contribution was thought to be small. For each sample examined, the backscattered fraction of the incident beam increased only a small amount over this energy range. From Fig. 1 of Ref. 20 I find 12±2 % of 1-keV positrons normally incident on Cu backscatter and 13±2 % of 5-keV positrons backscatter. Britton *et al.*[4] determined the fraction of epithermal energy positrons backscattered from clean Cu. Figure 2 of Ref. 4 shows the epithermal backscattered fraction is $\sim 4\%$ at 1-keV incident beam energy and decreases to $\sim 0\%$ at 5 keV. The combined results of these studies indicate the fraction of positrons backscattered from Cu is nearly constant ($\approx 14\%$) over the 1–5 keV energy range. Since Ni and Cu have similar densities and atomic numbers, it is reasonable to assume the fraction of positrons backscattered from Ni is the same as that for Cu. Accordingly, to account for the loss due to backscattering, the number of positrons implanted in the

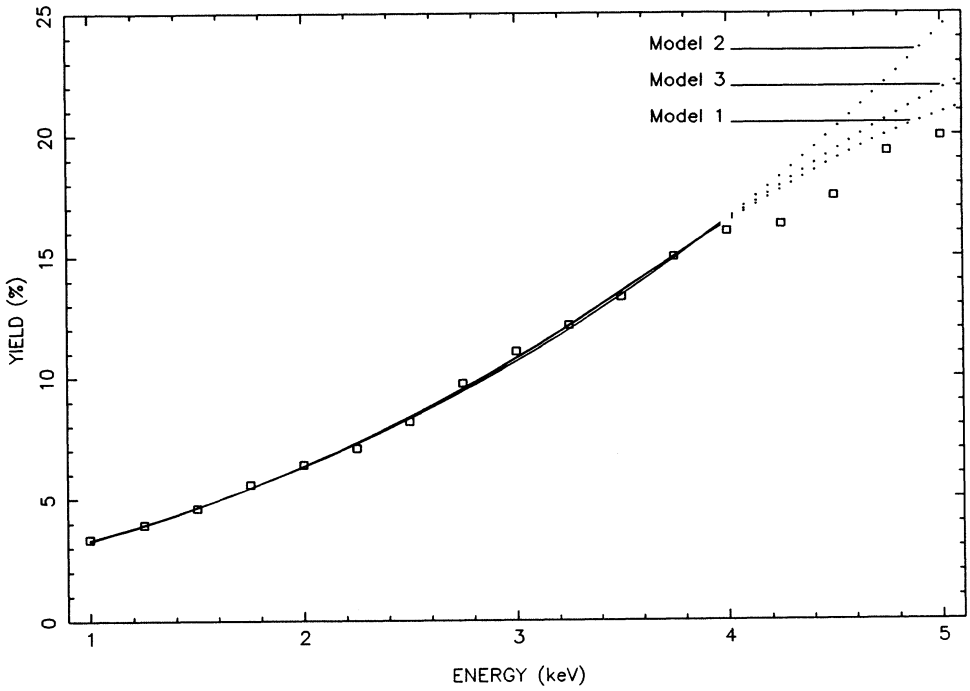

FIG. 2. $Y(E)$ measurement. Line shows best fit for models 1–3 (see discussion in text). The small reduction in yield at $E=4.25$ and 4.5 keV is attributed to the beam illuminating a defected area.

crystal was reduced by 14% (for all incident energies) when calculating the yield.

The effect of varying the implantation profile parameters, α, m, and n and the diffusion-sample parameters D_+, w, and $\mathcal{R}$ was examined by comparing the calculated and measured $Y(E)$. Only those parameters which affected the shape of the $Y(E)$ curve were kept free when the fits to the data were performed. Since the PRM cannot discriminate between thermal and nonthermal positrons when not being used to form a sharply focused high-magnification image, I chose to examine and fit only the data taken over the energy range for which the emitted nonthermal fraction was small; that is, $E \leq 4$ keV.[12] The calculations show that, over this energy range, the shape of the curve is insensitive to the diffusion constant (Fig. 3) and only the yield changes with the choice of D_+. Similarly, the sample width (w), which was varied between 1250 and 1750 Å, affected only the yield and not the curve shape. The remaining calculations were performed with $D_+ = 1.6$ cm^2 s^{-1} (Ref. 23) (see discussion in previous paper) and with the measured width $w = 1500$ Å. The variation of the implantation profile parameters α, m, and n all affected the shape of the curve. The choice of reflection coefficient $\mathcal{R}$ was also found to have a large effect on the shape of the curve (Fig. 4). Moreover, it was the only parameter among those investigated which effectively increased the yield at low implantation energy relative to the high implantation energy yield.

The initial fits to the data were done with the parameters α, m, n, and $\mathcal{R}$ free. Also kept free was a normalization (branching) constant f_{e+}, which gives the probability an emitted positron appears as a work function energy positron. A correlation between the positron implantation parameters α, m, and n was observed. Huomo

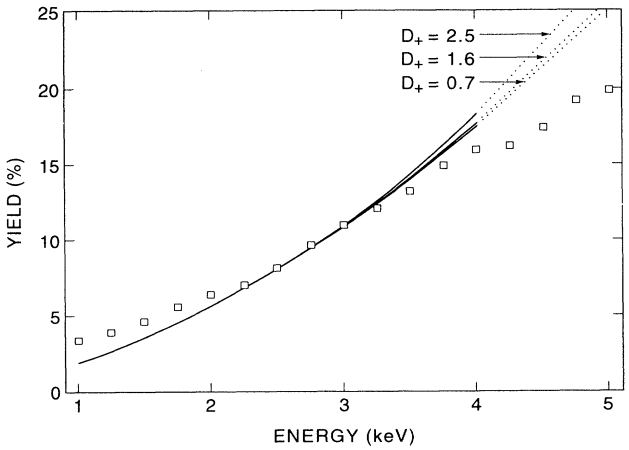

FIG. 3. Calculated $Y(E)$ for $D_+ = 0.7$, 1.6, and 2.5 cm^2 s^{-1}. For each calculation $m = 2.0$, $\mathcal{R} = 0.0$, $w = 1500$ Å, and $n = 1.6$. The calculated yields were normalized to the measured yield at $E = 2.5$ keV for comparison purposes.

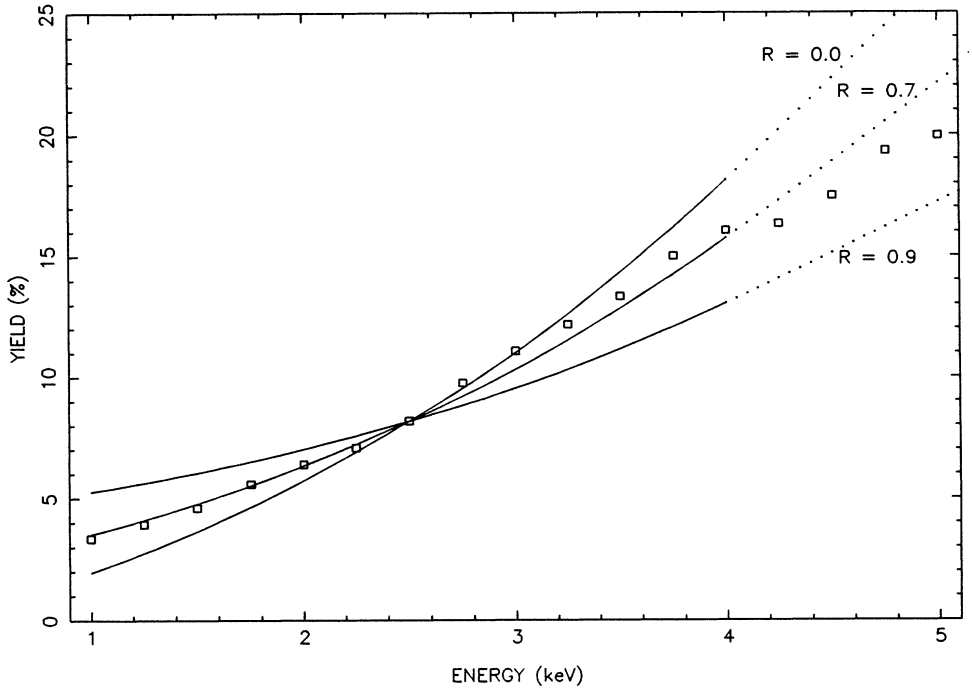

FIG. 4. Calculated $Y(E)$ for $\mathcal{R}=0.0$, 0.7, and 0.9. For each calculation $m=2.0$, $D_+=1.6\ \mathrm{cm^2\,s^{-1}}$, $w=1500$ Å, and $n=1.6$ The calculated yields were normalized to the measured yield at $E=2.5$ keV for comparison purposes.

et al.[24] suggested fixing

$$A=\alpha/\Gamma(1+m^{-1})=450/\rho\ \text{Å/keV}^n$$

to facilitate comparing experimental results from different labs. Most groups have measured or calculated $\alpha\approx 400/\rho$ Å/keV^n.[18,25,26] For these reasons I chose to fix $\alpha=400/\rho$ Å/keV^n, which yields $A\approx 450/\rho$ Å/keV^n for $1.3<m<5.0$.

The calculated yields and, consequently, the quality of the fits were found to be only weakly dependent on the shape parameter m. Unlike the back-reemission yield analysis of Huomo *et al.*, there was no correlation observed between the parameters m and n. For these reasons, and to limit the amount of computer time required for the fits, a shape parameter value m was chosen ($1.0\le m\le 2.5$) and fits with three free parameters (n, $\mathcal{R}$, and f_{e^+}) were performed. The results of the fits for $m=1.4$, which gave the lowest χ^2/ν, and for the frequently used shape parameter $m=2.0$ are presented in Table I.

Although for $E\le 4$ keV the transmitted nonthermal fraction was expected to be negligible relative to the slow positron yield, the effect of a nonthermal positron contribution to the slow positron yield was included. Three models of the nonthermal positron contribution to the slow positron yield were considered. In the first case (model 1), it was assumed that only thermal reemitted positrons were counted in the experiment (none of the transmitted nonthermal positrons reach the PRM detector). In the second case (model 2), I assumed all transmitted nonthermal positrons struck the detector and that they were counted as efficiently as thermal reemitted positrons. The transmitted nonthermal positron fraction f_t is defined as

$$f_t=\int_w^\infty P(z,E)dz\ , \tag{3}$$

TABLE I. Results of fitting calculated positron yields to the measured positron yields. Models 1–3 are described in the text.

	$m=1.4$			$m=2.0$		
	model 1	model 2	model 3	model 1	model 2	model 3
$\mathcal{R}$	0.63(4)	0.64(4)	0.63(4)	0.63(3)	0.63(4)	0.63(4)
n	1.61(3)	1.60(3)	1.61(3)	1.62(3)	1.61(3)	1.62(3)
f_{e^+}	0.68(3)	0.67(3)	0.68(3)	0.68(3)	0.68(3)	0.67(3)
χ^2/ν	20/10	26/10	21/10	27/10	27/10	26/10

where w is the crystal width. The small increase in f_t and the equivalent decrease in the implanted positron fraction near the $z=w$ surface, brought about by the absence of material beyond this boundary to scatter positrons back into the crystal, has been neglected. Using an electron trajectory program,[27] the PRM imaging efficiency was calculated to be $\sim 25\%$ for particles emitted isotropically and with energies greater than 20 eV. In the third case (model 3) I assumed 25% of the transmitted nonthermal positrons struck the PRM detector and that they were counted as efficiently as thermal positrons. The best fits obtained using each of these methods for counting the nonthermal positron contribution to the slow positron yields are given in Table I. Figure 2 shows the data and a comparison of the calculated $Y(E)$ curves for models 1–3. The similarity of the fit results for each model (Table I) support the assertion that the nonthermal fraction is insignificant below $E=4$ keV. From the results shown in Table I, I conclude that, for Ni(100), the reflection coefficient is $\mathcal{R}=0.63(4)$, $n=1.61(4)$, and $f_{e^+}=0.68(3)$. A fit to the 1.024–5.024 keV, 2-mm-diam collimator, rastered positron beam data of Schultz *et al.*[12] yielded $\mathcal{R}=0.87(1)$, $n=1.59(1)$, and $f_{e^+}=0.54(1)$ ($m=1.4$, $\alpha=400$, and $\chi^2/\nu=1963/13$).

IV. DISCUSSION OF RESULTS

A calculation of the size of the reflection coefficient using the one-dimensional potential step model of Britton *et al.* gives $\mathcal{R}=0.65$ [$\phi_+=1.1$ eV (Ref. 12)]. Calculating $\mathcal{R}$ with a potential well added to the potential step results in a value of $\mathcal{R}$ which is slightly larger than the potential step value, the exact size depending on the well dimensions. The good agreement between the measured $\mathcal{R}$ and the calculated results suggests that the size of the reflection coefficient depends more on the magnitude of the potential step than on the shape of the surface potential. Additional measurements from materials having different work functions and at different temperatures would help to confirm this statement.

It would be preferable to make measurements in the future with the capability to energy analyze the reemitted positrons. A grid which may be biased and moved in front of the sample once the microbeam has been tuned might be one way to accomplish this. A separate measurement of the thermal and nonthermal yields over a larger energy range would not only increase the precision with which $\mathcal{R}$ would be determined, but would remove the ambiguity in the choice of m.

It is interesting to ask how much a nonzero reflection coefficient will affect back reemitted e^+ and Ps yield measurements. Figure 5 shows the results of a numerical calculation of the positron yield ($f_{e^+}=1$) from a semi-infinite crystal versus implantation energy for various choices of R. The shape of the $Y(E)$ curves is similar but the yield is increasingly reduced as $\mathcal{R}$ is increased. Consequently, E_0, the incident positron energy (E) at which the yield (Y) is half the yield obtained for $E=0$, will be unchanged by a nonzero reflection coefficient. Similarly, parameters related to E_0, such as the mean diffusion length or the diffusion constant, will also be unchanged.[1]

The fraction of positrons emitted as slow positrons

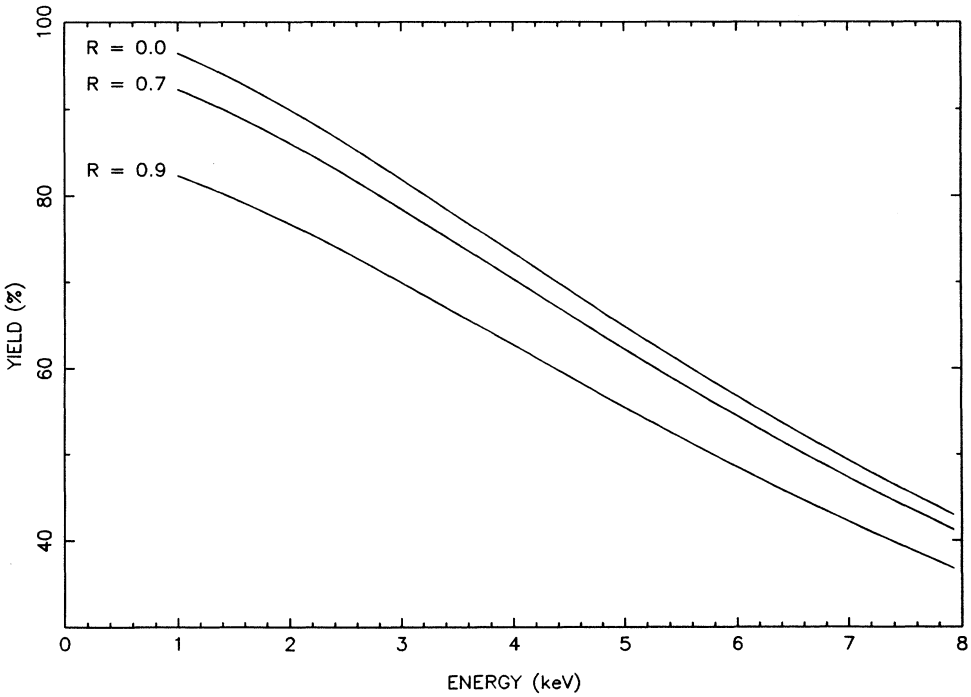

FIG. 5. Numerical calculation of the back-reemitted positron yield from a semi-infinite Ni crystal for $\mathcal{R}=0.0$, 0.7, and 0.9.

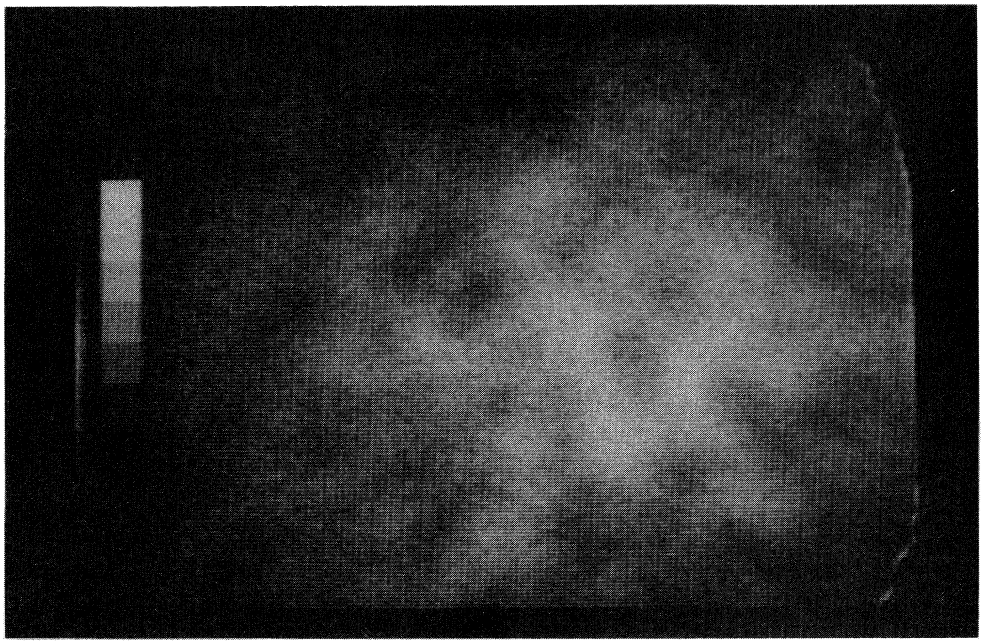

FIG. 6. PRM image of the Ni(100) sample at 4400×. The image acquisition time was 12 h. The brightest level of the eight level grey scale bar at the left of the image corresponds to 176 counts/pixel, the darkest to 22 counts/pixel. For purposes of scale, the grey scale bar is 400 nm×3200 nm. Assuming uniform illumination, the central dark areas emit slow positrons ~80% as efficiently as the central bright areas.

$[f_{e^+}=0.68(3)]$ is higher than that found by Gullikson *et al.*[28] $[f_{e^+}=0.45(5)]$. The discrepancy is attributed to differences in surface conditions. A high magnification PRM image of this foil (see Fig. 6) showed that the sample does not emit positrons with uniform efficiency. No evidence of surface roughness, which could account for the nonuniform emission intensity, was evident in an optical microscope examination of the Ni foil. These results suggest that still higher yields ($f_{e^+}\approx 0.75$) from Ni may be feasible if the entire foil emitted positrons as efficiently as the brightest areas in the image.

In conclusion, I have shown that a straightforward analysis of the transmitted slow positron yield from a thin single crystal versus implantation energy may be used to determine the magnitude of the positron reflection coefficient. The measurement of the reflection coefficient is in agreement with the value calculated from the one-dimensional potential step model.

ACKNOWLEDGMENTS

I would like to acknowledge the many helpful discussions I have had with K. F. Canter, A. P. Mills, S. Berko, K. Lynn, and H. Huomo. The assistance of T. Roach and Lasertron is gratefully acknowledged. This work is supported in part by National Science Foundation (NSF) Grant No. DMR 8820345.

*Present address: AT&T Bell Laboratories, Murray Hill, NJ 07974.

[1]P. J. Schultz and K. G. Lynn, Rev. Mod. Phys. **60**, 701 (1988).

[2]A. P. Mills, Jr., in *Positron Solid-State Physics,* edited by W. Brandt and A. Dupasquier (North-Holland, Amsterdam, 1982), p. 432.

[3]K. G. Lynn, in *Positron Solid-State Physics,* edited by W. Brandt and A. Dupasquier (North-Holland, Amsterdam, 1982), p. 609.

[4]D. T. Britton, P. A. Huttunen, J. Mäkinen, E. Soininen, and A. Vehanen, Phys. Rev. Lett. **62**, 2413 (1989), and references therein.

[5]J. B. Pendry, J. Phys. C **13**, 1159 (1980).

[6]R. M. Nieminen and J. Oliva, Phys. Rev. B **33**, 472 (1981).

[7]D. M. Chen, K. G. Lynn, R. Pareja, and B. Nielsen, Phys. Rev. B **31**, 4123 (1985).

[8]G. R. Brandes, K. F. Canter, T. N. Horsky, P. H. Lippel, and A. P. Mills, Jr., J. Phys.: Condens. Matter **1**, SA135 (1989).

[9]L. D. Hulett, J. M. Dale, and S. Pendyala, Mater. Sci. Forum **2**, 133 (1984).

[10]G. R. Brandes, K. F. Canter, and A. P. Mills, Jr., Phys. Rev. Lett. **61**, 492 (1988).

[11]J. Van House and A. Rich, Phys. Rev. Lett. **61**, 488 (1988).

[12]P. J. Schultz, E. M. Gullikson, and A. P. Mills, Jr., Phys. Rev. B **34**, 442 (1986).

[13]Single-crystal thin films are available from J. Chevallier, Uni-

versity of Aarhus, DK8000, Aarhus, Denmark.
[14]The foil thickness was measured with a Sloan Dektak II (Veeco Instr. Inc., Sloan Tech. Div., Santa Barbara, CA 93103).
[15]J. L. Wiza, Nucl. Instrum. Methods **162**, 587 (1979).
[16]K. G. Lynn, C. L. Snead, Jr., and J. J. Hurst, J. Phys. F **10**, 1753 (1980).
[17]A. F. Makhov, Fiz. Tverd. Tela (Leningrad) **2**, 2161 (1960) [Sov. Phys. Solid State **2**, 1934 (1960)]; **2**, 2172 (1960) [**2**, 1942 (1960)]; **2**, 2176 (1960) [**2**, 1945 (1960)].
[18]S. Valkealahti and R. M. Nieminen, Appl. Phys. A **35**, 51 (1984).
[19]W. H. Press, B. P. Flannery, S. A. Teukolsky, and W. T. Vetterling, *Numerical Recipes,* 1st ed. (Cambridge University, New York, 1986).
[20]J. A. Baker and P. G. Coleman, J. Phys. C **21**, L875 (1988).
[21]R. H. Howell, I. J. Rosenberg, and M. J. Fluss, Phys. Rev. B **34**, 3069 (1986).
[22]H. Huomo, A. Vehanen, M. D. Bentzon, and P. Hautojärvi, Phys. Rev. B **35**, 8252 (1987).
[23]A. Vehanen, K. G. Lynn, P. J. Schultz, E. Cartier, H.-J. Güntherodt, and D. M. Parkin, Phys. Rev. B **29**, 2371 (1984).
[24]H. Huomo, E. Soininen, and A. Vehanen, Appl. Phys. A **49**, 647 (1989).
[25]A. P. Mills, Jr. and R. J. Wilson, Phys. Rev. A **26**, 490 (1982).
[26]A. Vehanen, K. Saarinen, P. Hautojärvi, and H. Huomo, Phys. Rev. B **35**, 4606 (1987).
[27]Stanford Linear Accelerator Center (SLAC) Electron Trajectory Program, W. B. Hermannsfeldt, SLAC Report No. SLAC-226 (1978) (unpublished).
[28]E. M. Gullikson, A. P. Mills, Jr., and C. A. Murray, Phys. Rev. B **38**, 1705 (1988).

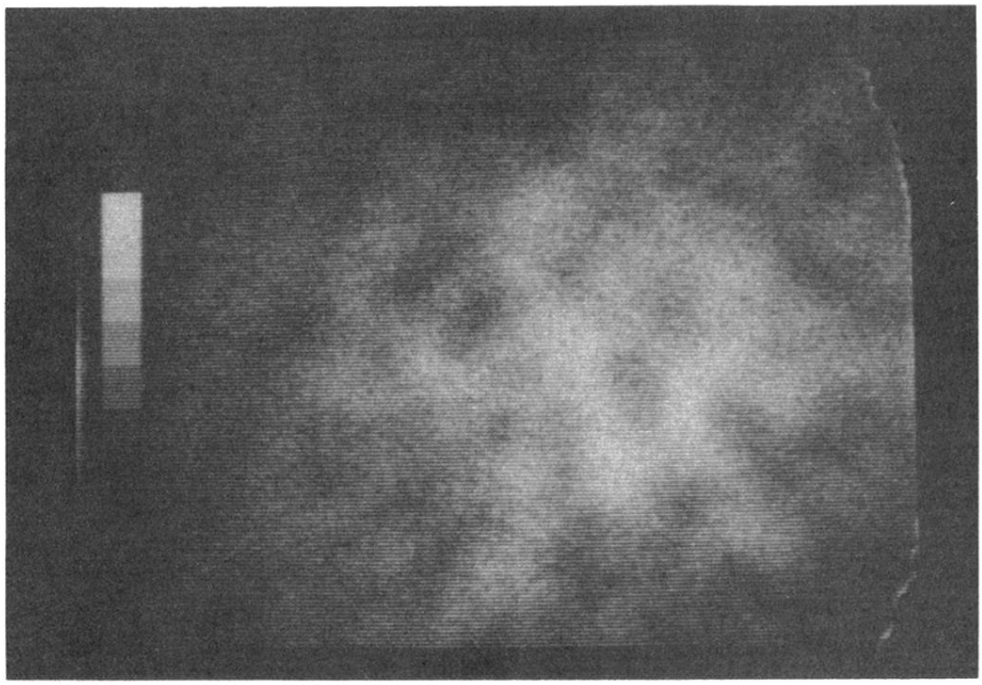

FIG. 6. PRM image of the Ni(100) sample at 4400×. The image acquisition time was 12 h. The brightest level of the eight level grey scale bar at the left of the image corresponds to 176 counts/pixel, the darkest to 22 counts/pixel. For purposes of scale, the grey scale bar is 400 nm×3200 nm. Assuming uniform illumination, the central dark areas emit slow positrons ~80% as efficiently as the central bright areas.